Cellular and Molecular Life Sciences (2019) 76:4783–4794
https://doi.org/10.1007/s00018-019-03133-1

ORIGINAL ARTICLE

PGAM5 is a key driver of mitochondrial dysfunction in experimental lung fibrosis

Ingo Ganzleben[1] · Gui-Wei He[1] · Claudia Günther[1] · Elena-Sophie Prigge[2,3] · Karsten Richter[4] · Ralf J. Rieker[5] · Dimitrios Mougiakakos[6] · Markus F. Neurath[1] · Christoph Becker[1]

Received: 8 January 2019 / Accepted: 6 May 2019 / Published online: 5 June 2019

Abstract

Rationale Mitochondrial homeostasis has recently emerged as a focal point in the pathophysiology of idiopathic pulmonary fibrosis (IPF), but conflicting data have been reported regarding its regulation. We speculated that *phosphoglycerate mutase family member 5* (PGAM5), a mitochondrial protein at the intersection of multiple cell death and mitochondrial turnover pathways, might be involved in the pathogenesis of IPF.

Methods PGAM5-deficient mice and human pulmonary epithelial cells were analyzed comparatively with PGAM5-proficient controls in a bleomycin-based model of pulmonary fibrogenesis. Mitochondria were visualized by confocal and transmission electron microscopy. Mitochondrial homeostasis was assessed using JC1 ($\Delta\Psi$) and flow cytometry.

Results PGAM5 plays an important role in pulmonary fibrogenesis. *Pgam5−/−* mice displayed significantly attenuated lung fibrosis compared to controls. Complementary, in vitro studies demonstrated that PGAM5 impaired mitochondrial integrity on a functional and structural level independently of mtROS-production. On a molecular level, reduced mitophagy caused by PGAM5 deficiency improved mitochondrial homeostasis.

Conclusions Our study identifies PGAM5 as an important regulator of mitochondrial homeostasis in pulmonary fibrosis. Our data further indicate PGAM5-mediated mitophagy itself as a pivotal gateway event in the mediation of self-sustaining mitochondrial damage and membrane depolarization. Our work hereby highlights the importance of mitochondrial dynamics and identifies a potential therapeutic target that warrants further studies.

Graphical abstract

Toxic agents lead to mitochondrial damage resulting in depolarization of the mitochondrial membrane potential ($\Delta\Psi$) which is a gateway event for the initiation of PGAM5-mediated mitophagy. PGAM5-mediated mitophagy in turn leads to

✉ Christoph Becker
christoph.becker@uk-erlangen.de

1 Department of Medicine 1, University Hospital, Friedrich-Alexander-Universität Erlangen-Nürnberg, Erlangen, Germany

2 Department of Applied Tumor Biology, Institute of Pathology, University Hospital Heidelberg, Heidelberg, Germany

3 Clinical Cooperation Unit Applied Tumor Biology, German Cancer Research Center (DKFZ), Heidelberg, Germany

4 Central Unit Electron Microscopy, German Cancer Research Center (DKFZ), Heidelberg, Germany

5 Department of Pathology, University Hospital, Friedrich-Alexander-Universität Erlangen-Nürnberg, Erlangen, Germany

6 Department of Medicine 5, University Hospital, Friedrich-Alexander-Universität Erlangen-Nürnberg, Erlangen, Germany

a self-perpetuating escalation of ΔΨ depolarization. Loss of the mitophagy-based damage-enhancing loop under PGAM5-deficient conditions breaks this vicious cycle, leading to improved mitochondrial homeostasis.

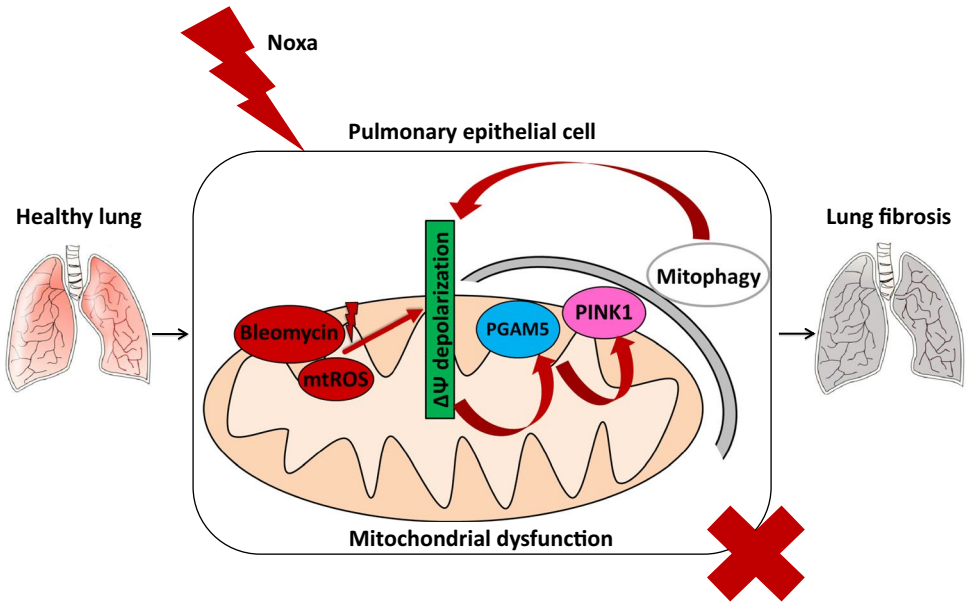

Keywords Mitophagy · Bleomycin · IPF

Introduction

Idiopathic pulmonary fibrosis has an infaust prognosis with dismal median survival after diagnosis [1]. As of today no curative therapy exists, underscoring the paramount importance of facilitating novel treatment concepts. Recently, autophagic processes have been implicated in the pathogenesis of IPF and various other pulmonary diseases [2, 3]. Autophagy is the capacity of cells to degrade damaged, dysfunctional, or otherwise dispensable structures, e.g., organelles by targeted double-membrane enclosure and degradation. Mitophagy, a particular subform of autophagy, specifically targets mitochondria [4]. Beneficial or detrimental consequences depend heavily on the context such as a given disease or a particular cell type [2, 3]. A recent study, for example, demonstrated a detrimental role of mitophagy initiated by (*PTEN*)-*induced putative kinase 1* (PINK1), a central regulator of mitophagy, in the pathogenesis of chronic obstructive pulmonary disease (COPD) [5]. Along the same lines, there is evidence for a pathogenic role of mitophagy in IPF by promoting the survival of pro-fibrotically polarized alveolar macrophages, thereby facilitating fibrosis [6]. In contrast, other studies have described substantial beneficial effects of mitophagy in IPF with a deficiency leading to aggravated pulmonary fibrosis [7, 8]. These inconsistent data underscore the need to further elucidate the mechanisms regulating mitophagy to better understand its multifaceted role in pulmonary diseases.

The mitochondrial protein *phosphoglycerate mutase family member 5* (PGAM5) has been identified as a convergence point of multiple necrotic cell death pathways. Moreover, it has been implicated in mitochondrial turnover, although its function in this context is not well understood. With old age, PGAM5-deficient mice develop a spontaneous Parkinson-like phenotype connected to reduced rates of mitophagy [9]. However, the consequences of PGAM5-mediated processes appear to be highly context sensitive. While it has been reported that PGAM5 exerted a protective effect in a model of ischemic–reperfusion injury in the heart and brain tissue with a beneficial effect of mitophagy being attributed as the molecular mechanism [10], PGAM5 has proved to be an indispensable mediator of experimental autoimmune hepatitis with evidence that mitochondrial fission plays an important role in this context [11]. A very recent study, has further demonstrated that PGAM5 plays a role in ozone damage and viral infection in the lung [12]. However, insights into the role of PGAM5 in chronic pulmonary diseases such as IPF are currently lacking. Given the importance of mitochondria in the pathogenesis of inflammatory and fibrotic pulmonary diseases [13], we decided to investigate the role of the mitochondrial protein PGAM5 in the pathogenesis of pulmonary fibrosis. We

hypothesized that PGAM5 might play a major role in the pathophysiology of lung fibrosis via its role as a regulator of mitochondrial dynamics.

Results

PGAM5 is an important mediator of experimental pulmonary fibrosis in vivo

We comparatively challenged PGAM5 knock-out (*Pgam5−/−*) and control mice using an established murine pulmonary fibrosis model of topical bleomycin administration (Fig. 1a). The extent of pulmonary alterations in the bleomycin-treated *Pgam5−/−* mice and the bleomycin-treated control mice was assessed during the experiment by longitudinal computed tomography (CT) imaging of the lung at days 7 and 21. Bleomycin-treated *Pgam5−/−* mice consistently displayed a reduction of pathologies on CT compared to bleomycin-treated controls reflecting reduced pulmonary infiltrates and consolidations both during the inflammatory phase (day 7) and the fibrotic phase (day 21) after bleomycin application (Fig. 1b). This protective phenotype was validated by histological assessment of the lungs comparing

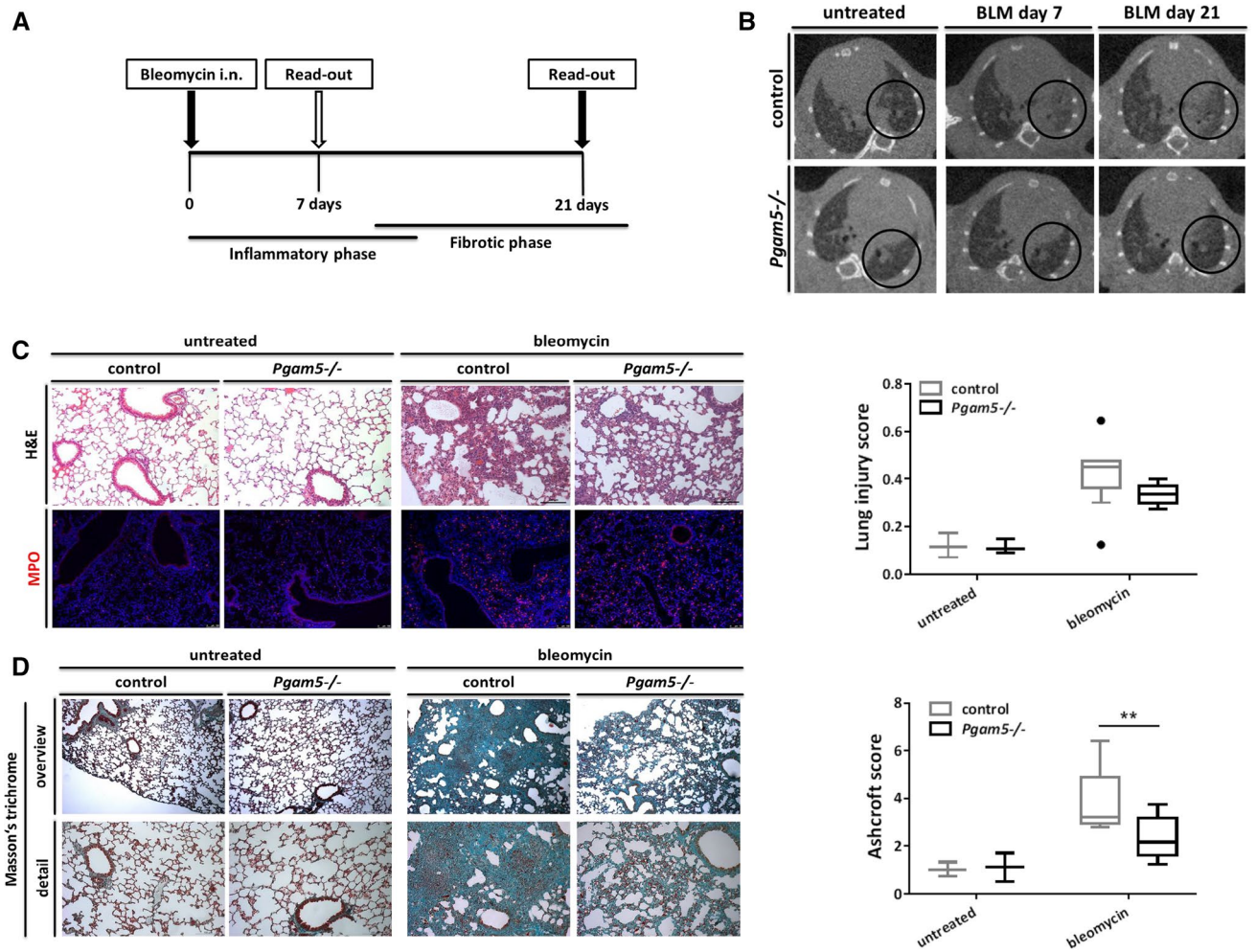

Fig. 1 PGAM5 is an important mediator of experimental pulmonary fibrosis in vivo. **a–d** *Pgam5−/−* and control mice were challenged with intranasal bleomycin and analyzed after 7 days ($n=12$ *Pgam5−/−* bleomycin; $n=12$ controls bleomycin) and 21 days ($n=13$ *Pgam5−/−* bleomycin; $n=10$ controls bleomycin). Each time point represents three independent experiments with similar results. Unchallenged mice ($n=3$ *Pgam5−/−*; $n=3$ controls) served as reference for both time points. **a** Model of bleomycin-induced pulmonary inflammation and fibrosis. **b** CT of the lung with cross sections of comparable anatomical locations. Healthy lung tissue is black, and diseased lung tissue increasingly white (increased density). **c** Representative H&E and MPO immunofluorescence (IF) staining of lung tissue 7 days after bleomycin treatment. Bar 100 µm. Quantitative lung injury score as Tukey box plot. One-way ANOVA with Tukey's test ($p=0.11$). **d** Representative Masson's trichrome staining (overview: bar 100 µm; detail: bar 200 µm) with quantitative histological fibrosis scoring (Ashcroft score) of lung tissue 21 days after bleomycin. Tukey box plot. One-way ANOVA with Tukey's test (**$p<0.01$ *Pgam5−/−* bleomycin compared to control bleomycin)

treated *Pgam5−/−* and treated control mice at day 7 (Fig. 1c) and day 21 (Fig. 1d). Accordingly, we assessed neutrophil infiltration, signs of epithelial barrier defects, and structural damage by a previously described weighted composite score in consultation with a pulmonary pathologist, revealing that structural damage of the pulmonary architecture and inflammatory changes of the lung were reduced in *Pgam5−/−* mice compared to controls at day 7 (Fig. 1c). Strikingly, at day 21, *Pgam5−/−* mice displayed significantly reduced overall fibrotic changes and reduced architectural damages of the lung. This was evidenced by assessment of structural alterations and collagen deposits using Masson's trichrome staining (Fig. 1d). In particular, *Pgam5−/−* mice had quantitatively reduced fibrotic obliteration as well as reduced alveolar thickening compared to bleomycin-treated control animals. This significant fibrosis reduction in *Pgam5−/−* mice was confirmed by statistical analysis of the established Ashcroft score (Fig. 1d). In summary, our in vivo findings for the first time suggested PGAM5 as an important player in inflammatory fibrogenesis of the lung.

PGAM5 drives bleomycin-induced cytotoxicity and mitochondrial dysfunction in human pulmonary epithelial cells

To support our functional in vivo observations and study the effects of PGAM5 on a cellular level, we generated PGAM5-deficient A549 pulmonary epithelial cells (A549 PGAM5-KO) using the CRISPR/Cas9 system and comparatively analyzed them and A549 cells in an in vitro bleomycin model using two concentrations of bleomycin (100 µg/ml and 200 µg/ml) and variable time intervals of up to 48 h.

Untreated A549 and A549 PGAM5-KO cells displayed comparable continuous growth during the observational period (48 h) evidenced by an increasing normalized cell index (NCI) in the Xcelligence real-time cell analyzer (Fig. 2a). Bleomycin induced a marked NCI decrease over time in A549 cells. In contrast, A549 PGAM5-KO cells displayed a protected phenotype evidenced by a significantly reduced NCI decrease compared to their bleomycin-treated wild-type counterparts (Fig. 2a). This reflected a reduced cytotoxicity in the PGAM5-deficient cells under bleomycin treatment. In line with these findings, light microscopy after 48 h also revealed a protective phenotype of the PGAM5-deficient cells against bleomycin, as evidenced by increased cellular density and reduced morphological alterations when compared to wild-type controls (Fig. 2b left panel).

In a next step, we utilized reconstitution experiments to confirm that the observed protective phenotype was indeed causally determined by the deficiency of PGAM5 in our cells. Accordingly, we transiently expressed full-length PGAM5 in A549 PGAM5-KO cells. The expression of PGAM5 in PGAM5-deficient A549 cells reconstituted susceptibility of these cells toward the noxious effects of bleomycin (Fig. 2b right panel). Bleomycin-treated PGAM5-expressing A549 PGAM5-KO cells displayed a morphological phenotype similar to that of bleomycin-treated A549 cells after 48 h (Fig. 2b). In summary, A549 PGAM5-KO cells proved to be more resilient to bleomycin treatment than their wild-type counterparts. Absence of PGAM5 in A549 PGAM5-KO cells as well as effective PGAM5 expression in the reconstitution experiments was confirmed by immunoblotting (Fig. 2c). In a next step, we assessed the implications of PGAM5 for basic mitochondrial functions such as mitochondrial membrane potential ($\Delta\Psi$) integrity. To analyze changes in $\Delta\Psi$, we used a JC-1 dye-based immunofluorescence staining. JC-1 forms aggregates in cells with an intact $\Delta\Psi$, emitting a red fluorescence signal. In line with our hypothesis, A549 cells displayed increasing mitochondrial depolarization after bleomycin treatment over time, evidenced by increasing persistence of non-aggregated JC-1 monomers emitting a green fluorescence signal after 48 h (Fig. 2d). Strikingly, mitochondrial depolarization was significantly reduced in bleomycin-treated A549 PGAM5-KO cells in comparison to their wild-type counterparts (Fig. 2d). Of note, similar results could be obtained using PGAM5-deficient human lung epithelial cells (BEAS-2B; data not shown).

Pertinently, genetically PGAM5-deficient cells with transient vector-based PGAM5 expression also displayed a restored susceptibility toward bleomycin treatment with quantitatively increased $\Delta\Psi$ depolarization when compared to PGAM5-deficient controls after 48 h (Fig. 2e).

PGAM5 mediates structural damage of mitochondria in human pulmonary epithelial cells after bleomycin treatment

Interestingly, microscopic analysis of PGAM5 localization in A549 cells after bleomycin treatment revealed that PGAM5 organized into granular structures and increasingly localized to the perinuclear region over the course of 48 h corresponding to a typical mitochondrial damage pattern (Fig. 3a). Therefore, we evaluated the topographic relationship of PGAM5 to the structural mitochondrial marker *translocase of outer mitochondrial membrane 20* (*TOMM20*) under these conditions. Confocal microscopy demonstrated that PGAM5 predominantly co-localized with TOMM20 in this context, supporting the notion that PGAM5 remained localized to the mitochondria during the course of bleomycin-induced mitochondrial damage (Fig. 3b). Quantitative assessment of TOMM20 further revealed a time and bleomycin-dose dependent phenotype of a polar perinuclear consolidation in PGAM5-proficient cells after bleomycin treatment. In contrast, this morphological phenotype was significantly less prevalent in

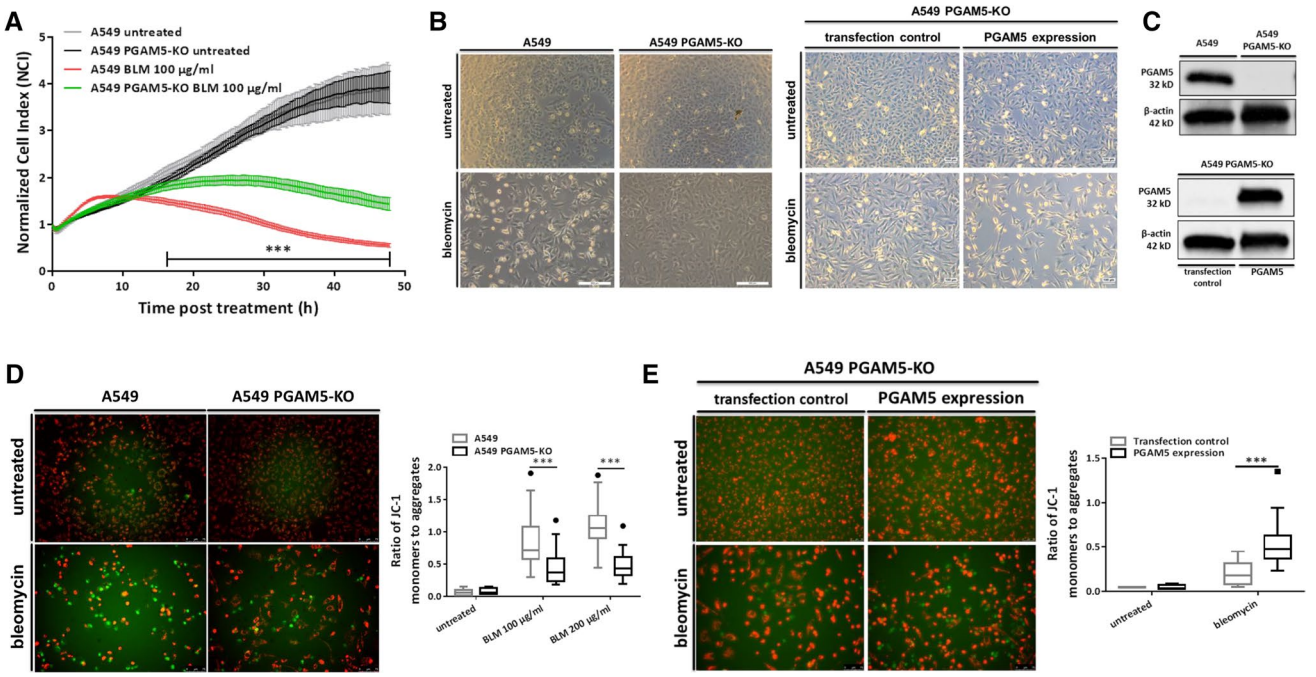

Fig. 2 PGAM5 drives bleomycin-induced cytotoxicity and mitochondrial dysfunction in human pulmonary epithelial cells. A549 (**a**–**d**) and A549 PGAM5-KO (**a**–**e**) cells were treated either with bleomycin 100 µg/ml (**a, b, d, e**) or bleomycin 200 µg/ml (**d**) and analyzed over the course of 48 h (**a**), respectively, after an interval of 48 h (**b**, **d**, **e**). Depictions are representative of three independent experiments with similar results. Untreated cells of each modality served as controls. (**a**) X-celligence. Normalized cell index (NCI) normalized to the time of bleomycin addition. Each curve represents multiple measurements ($n=4$ for untreated, $n=6$ for treated modalities). Two-way ANOVA with Tukey's test (***$p<0.001$ comparing bleomycin-treated A549 PGAM5-KO to bleomycin-treated A549). Displayed are mean and error ± SD. **b** Light microscopy. Left panel: A549 and A549 PGAM5-KO cells (bar 500 µm). Right panel: A549 PGAM5-KO cells either transfected with a transfection control or with a PGAM5 plasmid to induce PGAM5 expression (bar 100 µm). **c** PGAM5 deficiency (upper panel) and efficient vector-based PGAM5-expression in genetically deficient A549 PGAM5-KO cells (lower panel) was confirmed using immunoblotting. β-Actin served as loading control. **d**, **e** JC-1 experiments: healthy cells (intact $\Delta\Psi$) emit a red signal (JC-1 aggregates). Cells with depolarized $\Delta\Psi$ emit a green signal (JC-1 monomers). An increased green-to-red-ratio indicates a higher percentage of depolarized cells. Graphs are Tukey box plots. **d** Representative JC-1 IF microscopy (bleomycin 100 µg/ml, bar 75 µm). Cumulative quantification: > 900 events per modality were assessed. Two-way ANOVA with Tukey's test (***$p<0.001$). **e** A549 PGAM5-KO cells were analyzed in comparison to A549 PGAM5-KO cells with vector-based PGAM5 expression (via transfected plasmid analogous to Fig. 2b and c) employing JC-1 IF microscopy. Representative JC-1 IF microscopy (upper panel: untreated, bar 50 µm; lower panel: bleomycin 100 µg/ml, bar 75 µm). Quantification: > 1500 events of each modality were assessed. Two-way ANOVA with Tukey's test (***$p<0.001$)

PGAM5-deficient cells reflecting a protective effect mediated by PGAM5 deficiency on a structural level (Fig. 3c). Interestingly, PGAM5 deficiency was additionally correlated with a pronounced reticular organization of the mitochondria under bleomycin treatment. To further investigate this finding, we performed transmission electron microscopy (TEM) (Fig. 3d). In doing so, we found that PGAM5-deficient mitochondria indeed predominantly formed an elongated, slender, and highly branched ultrastructural phenotype in response to bleomycin after 48 h, supporting our previous observations. They also displayed less pronounced membrane alterations compared to their wild-type counterparts. In contrast, PGAM5-proficient mitochondria frequently displayed irregularly bent cristae and showed signs of damage including mitochondrial swelling after bleomycin treatment (Fig. 3d).

PGAM5 disrupts mitochondrial function by mediating downstream mitophagy independently of mtROS levels

Next, we measured mtROS levels in vitro by mitoSOX-based flow cytometry analysis (Fig. 4a). While we found that bleomycin increased mtROS levels compared to untreated controls, there was no significant difference between bleomycin-treated A549 and bleomycin-treated A549 PGAM5-KO cells after 24 h (Fig. 4a).

In line with the occurrence of autophagy, bleomycin treatment led to an increased conversion of LC3B I to LC3B II in comparison to the respective controls after 24 h (Fig. 4b). Of note, the LC3B II/LC3B I ratio was reduced in bleomycin-treated A549 PGAM5-KO cells compared to their treated wild-type counterparts (Fig. 4b). These

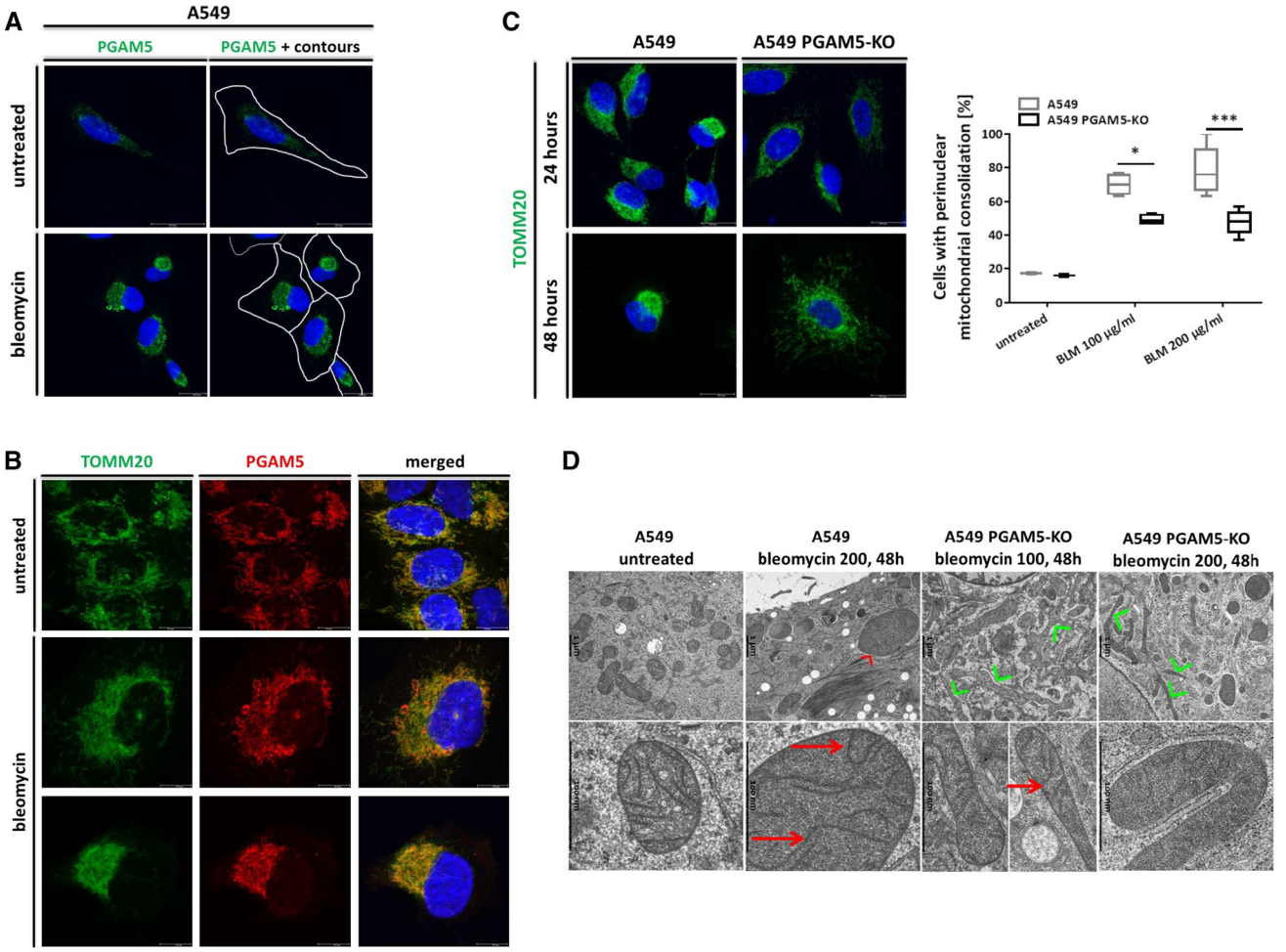

Fig. 3 PGAM5 mediates structural damage of mitochondria in human pulmonary epithelial cells after bleomycin treatment. A549 and A549 PGAM5-KO cells were treated with bleomycin 100 µg/ml (**a**, **c**, **d**) or bleomycin 200 µg/ml (**b**, **c**, **d**) for 48 h unless stated otherwise. Depictions are representative of three independent experiments (**a**, **c**), one iteration per time point (**b**, 24 h results not shown) or one measurement series (**d**) with similar results. Nuclei were counterstained with Hoechst 33342. (**a**–**c**) Confocal immunofluorescence images (**a**) PGAM5. Right column: overlay of fluorescence images with cell contour outlines based on bright-field overlay (bar 20 µm; bright field not shown). (**b**) PGAM5 and TOMM20 co-localization (bar 10 µm). (**c**) TOMM20 visualization. Representative images of TOMM20 staining (bleomycin 100 µg/ml; 24 h, 48 h; bar 20 µm). Quantification (after 48 h): > 140 cells per modality were assessed. Tukey box plot. Two-way ANOVA with Tukey's test (*$p < 0.05$/***$p < 0.001$). **d** Independent TEM images. Overview (upper panel): arrowheads mark different mitochondrial subtypes: elongated/branched (green) and swollen (red). Details (lower panel): red arrows mark mitochondrial membrane alterations

data indicated that PGAM5 was involved in the increased autophagy observed in bleomycin-treated A549 cells. To focus more specifically on mitophagy, we isolated mitochondria from bleomycin-treated PGAM5-proficient and PGAM5-deficient A549 cells. Through this, we could demonstrate that bleomycin treatment led to an accumulation of LC3B II in the mitochondrial fraction with a marked increase of the LC3B II/LC3B I ratio suggesting the initiation of mitophagy (Fig. 4c). Interestingly, the detected increase in the LC3B II/LC3B I ratio was distinctively more pronounced compared to the results observed in our immunoblot analysis of whole cell lysate, suggesting events in the mitochondrial compartment to be the main determinant of these observed changes. Strikingly, the increase in the LC3B II/LC3B I ratio was significantly attenuated in the mitochondria of A549 PGAM5-KO cells compared to mitochondria of A549 cells after bleomycin treatment, suggesting reduced mitophagy initiation in PGAM5-deficient cells (Fig. 4c).

Next, we visualized PINK1 protein expression in PGAM5-proficient and PGAM5-deficient A549 cells after 24 h of bleomycin treatment. In doing so, we could observe a focal clustering of PINK1 resulting in a granular staining pattern. Importantly, this granular organization was markedly reduced in PGAM5-deficient cells (Fig. 4d). We reasoned that the spatial reorganization of the mitophagy

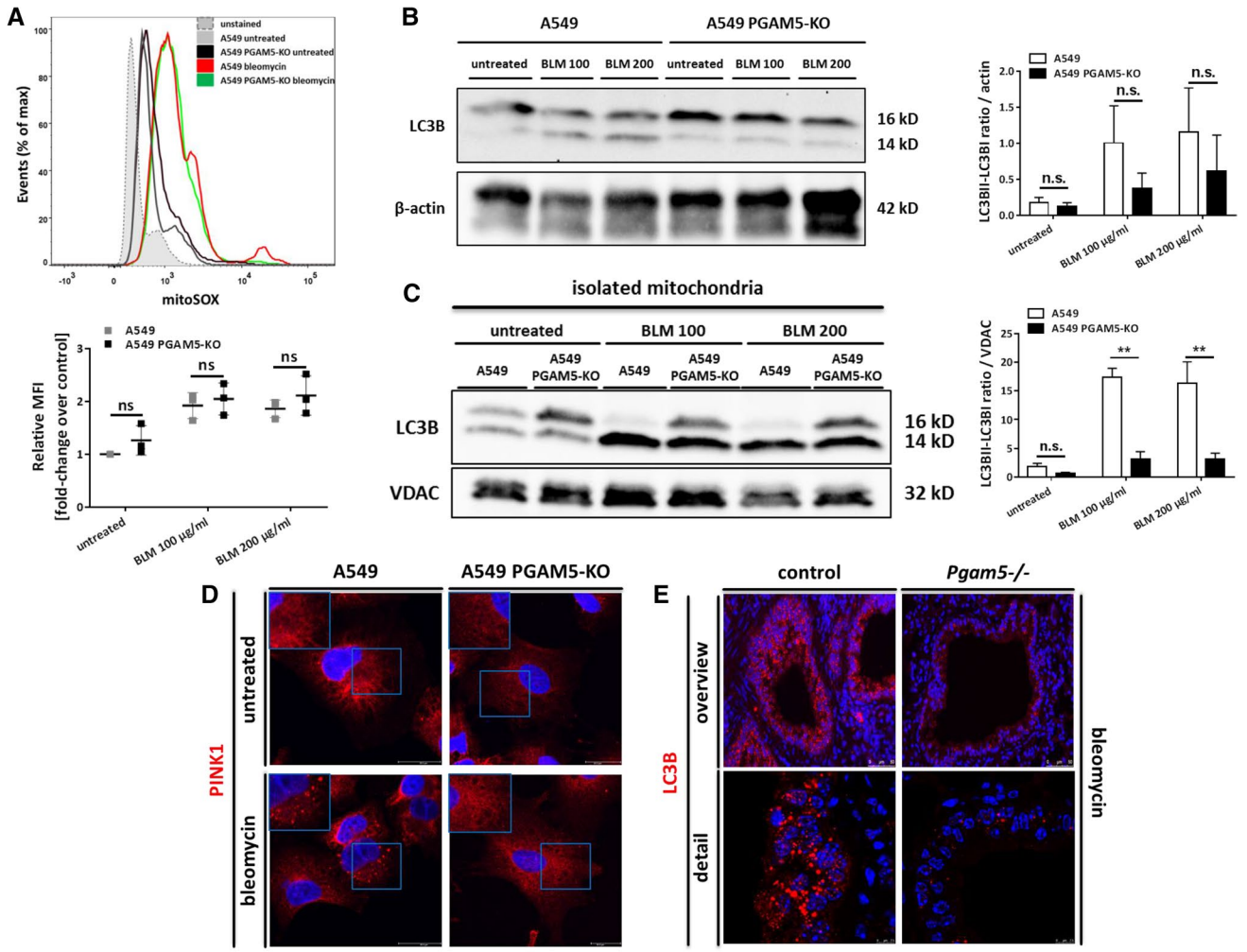

Fig. 4 PGAM5 disrupts mitochondrial function by mediating downstream mitophagy independently of mtROS levels. A549 and A549 PGAM5-KO cells (**a**–**d**) were treated with bleomycin 100 µg/ml (**a**–**d**) or bleomycin 200 µg/ml (**a**–**c**) and analyzed after 24 h. All results are representative of three independent experiments with similar results. Nuclei were counterstained with Hoechst 33342. **a** Mitochondrial ROS (mtROS) were measured by mitoSOX flow cytometry. Histogram: x-axis displays fluorescence signal intensity; *y*-axis displays events as percentage of the maximum. Graph: aligned dot plot with mean ± SD of relative mean fluorescence intensity (MFI). Two-way ANOVA (ns $p \geq 0.05$). Statistical analysis is cumulative. **b** Western blot from whole cell lysate with immunoblotting of LC3B. β-Actin served as loading control. Bar chart with mean and SEM displays the pooled densitometry results of the LC3BII–LC3BI ratio (lower and upper band, respectively) after normalization to β-actin [for each genotype (A549/A549 PGAM5-KO): $n = 2$ "untreated"; $n = 3$ "BLM 100 µg/ml"; $n = 2$ "BLM 200 µg/ml"]. Two-way ANOVA (ns $p \geq 0.05$). Statistical analysis is cumulative. **c** Western blot from isolated mitochondria with immunoblotting of LC3B. VDAC served as loading control. Bar chart with mean and SEM displays the pooled densitometry results of the LC3BII–LC3BI ratio (lower and upper band, respectively) after normalization to VDAC [for each genotype (A549/A549 PGAM5-KO): $n = 2$ "untreated"; $n = 3$ "BLM 100 µg/ml"; $n = 3$ "BLM 200 µg/ml"]. Two-way ANOVA with Tukey's test (ns $p \geq 0.05$/** $p < 0.01$). Statistical analysis is cumulative. **d** Confocal immunofluorescence images of PINK1 (bar 20 µm). **e** Immunofluorescence images of LC3B on murine lung sections of mice sacrificed 7 days after bleomycin challenge (same cohort as Fig. 1c). Scale bar 50 µm (upper panel, microscopy), scale bar 7.5 µm (lower panel, confocal microscopy)

mediator PINK1 reflected the initiation of mitophagic degradation facilitated by PGAM5-mediated PINK1 stabilization.

To finally confirm the relevance of these findings in vivo, we visualized LC3B in the lungs of challenged PGAM5-proficient and PGAM5-deficient mice after 7 days by immunofluorescence. During this initial phase, we found a clustering of LC3B indicating the initiation of autophagy in the early stage of inflammatory fibrogenesis. In accordance with our in vitro data, we observed a reduced clustering in bleomycin-challenged *Pgam5−/−* mice compared to challenged controls suggesting reduced autophagy in PGAM5-deficient mice (Fig. 4e).

Discussion

In summary, our study for the first time identifies PGAM5 as a novel player in the pathogenesis of pulmonary fibrosis acting by disruption of mitochondrial homeostasis.

So far, mitophagy has been proven to be a double-edged sword in pulmonary diseases with the outcome depending to a great extent on the context of its occurrence, e.g., the disease model [4, 13]. In recent publications that suggested a predominantly protective role of mitophagy in IPF and its murine model diseases, a reduction of mitophagy has been described to promote the development of pulmonary fibrosis [7, 8]. In those studies, PINK1 deficiency led to the accumulation of swollen and damaged mitochondria with detrimental consequences for the individual cell and the organism as a whole. These findings are in line with one basic theory of mitophagy as a way to eliminate and recycle damaged mitochondria to the benefit of the cell. Additionally, recent publications have described mitochondrial depolarization as a key event in the initiation of PGAM5/PINK1-mediated mitophagy to dispose of damaged and depolarized mitochondria [9, 14]. Given these observations, we had anticipated an accumulation of bleomycin-damaged mitochondria, as bleomycin exerts its damaging effects over a protracted period of time, leading to lung fibrosis. Therefore, the improved mitochondrial homeostasis in our model caused by PGAM5 deficiency was initially unexpected.

PGAM5 has been characterized not only as a mediator in mitophagy, but also in several cell death execution pathways with a significant overlap and convergence of both functions [11, 15]. The details of PGAM5 function, however, depend greatly on the specific context. In a very recent study, PGAM5 deficiency led to aggravated lung damage in in vivo models using acute noxa such as ozone exposure and virus infection [12]. The authors concluded that a PGAM5-mediated form of cell death termed "oxeiptosis" was necessary as a protective mechanism to prevent excessive inflammation and destruction of lung tissue as a whole in this setting. In oxeiptosis, PGAM5 acts as part of a central ROS-dependent cell death pathway independent of mitochondrial damage in particular and without evidence of autophagy [12]. Our data, however, uncover a new and complementary PGAM5 function in the setting of chronic pulmonary damage, highlighting the role of PGAM5 in mitochondrial homeostasis and quality control. In this context, direct mitochondrial damage is the key event causing mitochondrial membrane depolarization, subsequently triggering PGAM5-mediated mitophagy.

Surprisingly, our results not only demonstrated that PGAM5-deficient cells were more resistant to bleomycin as a whole and PGAM5 deficiency exerted a congruent protective effect on the integrity of mitochondrial function and structure, but also that blockage of mitophagic degradation led to improved mitochondrial homeostasis despite comparable initial bleomycin effects on the mitochondria. Previous studies have underscored the importance of initial mitochondrial damage and particularly mitochondrial ROS in experimental lung fibrosis [16]. Interestingly, we found that mtROS levels did not depend on the presence of PGAM5 in our model, leading us to reason that the main determinant of mtROS levels was indeed the direct induction through bleomycin action upstream and independent of PGAM5 function. In contrast, PGAM5 function proved necessary for mtROS induction in a widely different context in which extracellular matrix detachment and not primarily mitochondrial damage led to mitophagy-mediated cell death in a *Receptor-interacting serine/threonine-protein kinase 1* (RIP1)-mediated fashion [15]. These findings overall supported our notion of PGAM5-mediated mitophagy in lung fibrosis as a key event in the regulation of mitochondrial homeostasis, instead of a secondary event in a cellular cell death pathway. Our results regarding mitophagy were complemented by our observation of an ultrastructural phenotype of mitochondrial elongation that has previously been described as a protective mechanism under mitophagy-inducing conditions [17, 18] and has been associated with PGAM5 deficiency in a different context [19]. In light of these observations, we inferred that PGAM5 was an important mediator of bleomycin-induced structural mitochondrial damage. In line with the notion of breaking this vicious cycle by PGAM5 deficiency, we could demonstrate a correlation of reduced occurrence of mitophagy and improved mitochondrial homeostasis in PGAM5-deficient cells. Interestingly, observations connecting reduced mitophagy with increased stability of $\Delta\Psi$ have been made in the pathogenesis of COPD [5]. Yet, despite these new insights, the exact molecular mechanisms underlying these processes remain to be elucidated and will require further studies.

In conclusion, our current study for the first time characterizes PGAM5 as an important mediator in the pathogenesis of pulmonary fibrosis by facilitating mitophagy-mediated pathomechanisms.

Methods

Study approval

Animal protocols were approved by the Institutional Animal Care and Use Committee of the "Universität Erlangen-Nürnberg" and the government of Lower Franconia.

Animal model

Pgam5−/− mice were obtained from the International Knockout Mouse Consortium. Pulmonary inflammation

and fibrosis were induced in *Pgam5−/−* mice and age/sex-matched controls by onetime intranasal bleomycin application (BLEO-cell, Stada) in sterile PBS. Mice were anesthetized, carefully inoculated with 3 mg/kg body weight bleomycin, and sacrificed either 7 or 21 days post-bleomycin application. During the experiments, native CT of the lungs was performed at day 7 and day 21 ["Quantum FX μCT Imaging System" (Perkin Elmer)] under isoflurane anesthesia. Breathing artifacts were reduced by the μCT respiratory gating software protocol. Assessment of CT data was performed by blinded binary grading.

Cell culture

A549 epithelial cells were maintained in Dulbecco's Modified Eagle's Medium (DME)/Ham's Nutrient Mixture F-12 (D8062, Sigma-Aldrich) completed with 10% fetal bovine serum (10500, Gibco) and 1% penicillin/streptomycin (P4333, Sigma-Aldrich). Cells were repeatedly confirmed as mycoplasma negative by PCR (PCR Mycoplasma Test Kit A3744, Applichem). A549 cells were purchased from CLS Cell Lines Service GmbH (300114).

Cell culture models

A549 and PGAM5-deficient A549 PGAM5-KO cells were seeded in various formats and allowed to become adherent overnight. Cells were then stimulated with variable concentrations of bleomycin (100 μg/ml and 200 μg/ml) and studied for up to 48 hours with different read-out modalities. The specific bleomycin concentrations and time-points of study are detailed in the description of the respective experiments and their figure legends.

CRISPR/Cas9-mediated knockout of PGAM5 in vitro

A549 cells were transfected with the PGAM5 CRISPR/Cas9 KO Plasmid (h) (sc-401300, Santa Cruz) using Lipofectamine 2000 Transfection Reagent (11668019, Thermo Fisher Scientific) according to the manufacturer's protocol. Single clones were isolated using fluorescence activated cell sorting and tested for their PGAM5 status by immunofluorescence staining (PGAM5 antibody HPA036978, Sigma-Aldrich). After cell clone expansion, the successful knockout of PGAM5 was confirmed by immunoblotting.

Histology

Formalin-fixed and paraffin-embedded murine lung samples were cut into 3 μm thin histological sections and stained either according to Mayer's Hematoxylin & Eosin protocol or the Masson-Goldner-Trichrome protocol. Severity of inflammatory changes and tissue damage during the early phase was quantified using an established weighted scoring system for lung injury devised by the American Thoracic Society [20]. Quantification of fibrosis was performed using the Ashcroft score [21].

Image processing

Images of all microscopy samples were globally white-balanced, sharpened and adjusted for color-saturation and brightness to correctly represent the stained original slide (Adobe Photoshop CS5 extended).

Immunofluorescence

Cells were grown on 8-well culture slides (REF 354108, Falcon and 80826, ibidi). After completion of experimental procedures, cells were fixed according to the respective antibody-specific protocol, permeabilized with 0.1% Triton-X-100 solution and stained with the respective primary antibody as outlined below. Formalin-fixed paraffin-embedded lung tissue samples were deparaffinized and subsequently stained using a TSA Plus Cyanine 3 System (NEL744001KT, Perkin Elmer) according to the manufacturer's protocol with the respective primary antibody outlined below. Nuclei were counterstained with Hoechst 33342.

Primary antibodies used for in vitro and in vivo experiments: TOMM20 (HPA011562, Sigma-Aldrich), TOMM20 (ab56783, abcam), PGAM5 (HPA036978, Sigma-Aldrich), LC3B (3868, Cell Signaling Technologies), Myeloperoxidase (MPO) (ab139748, abcam), PINK1 (BC100-494, Novus Biologicals)

Secondary antibodies used: Goat anti-rabbit (111-065-144, Dianova), donkey anti-rabbit (Alexa Fluor 488, Cat A-21206, Thermo Fisher), donkey anti-rabbit (Alexa Fluor 555, Cat. 406412, BioLegend), donkey anti-mouse (DyLight 488, SA5-10166, Invitrogen).

Immunoblotting

Proteins were extracted either from whole cell lysate or mitochondrial fraction isolate of A549 and A549 PGAM5-KO cells using Cell Lysis Buffer (9803, Cell Signaling Technologies) with added Proteinase-Inhibitors (complete tablets mini, 04 693 159 001, Roche) and Phosphatase-Inhibitors (Phospho Stop, 04 906 837 001, Roche). Protein concentration was determined via Bradford Assay (Roti-Quant, K015.1, Carl Roth). Electrophoresis of denatured proteins was performed using appropriate 4–15% polyacrylamide Mini-Protean Tris-Glycine eXtended

Stain-Free (TGX) gels (Biorad). Proteins were transferred to a nitrocellulose membrane by semi-wet blotting. The membrane was probed with primary antibodies as listed below and proteins were visualized by Western Lightning Plus-ECL (NEL104001EA, Perkin Elmer) after probing with a HRP-linked antibody.

Primary antibodies: LC3B (3868, Cell Signaling Technologies), VDAC (D73D12, HRP-conjugate; 12454, Cell Signaling Technologies), PGAM5 (HPA036978, Sigma-Aldrich), β-actin (AC-15, HRP; ab49900, abcam)

Secondary antibodies: Anti-rabbit IgG, HRP-linked Antibody (7074, Cell Signaling Technologies)

Normalization and densitometry were performed with Image Lab software (Bio-Rad).

Microscopy

Microscopy imaging was performed using the Leica DMI4000 B microscope system employing either the Leica DFC420C color camera for bright-field or the Leica DFC360 FX fluorescence camera for fluorescence detection. Confocal microscopy was performed using the Leica TCS SP5 II confocal microscope system.

Mitochondrial membrane potential (ΔΨ) assessment (JC-1 dye)

Cells were grown on 8-well culture slides (REF 354108, Falcon and 80826, ibidi) and treated with either bleomycin 100 µg/ml, bleomycin 200 µg/ml or left untreated as controls. After 48 h, JC-1 staining was performed with the JC-1 Mitochondrial Membrane Potential Assay Kit (10009172, Cayman Chemicals) according to the manufacturer's protocol. Quantification was performed by counting the ratio of green to red signals of a sufficient cumulative number of events (specific numbers are outlined in the respective figure legends) using Fiji software [22]. An increased ratio reflects a higher percentage of depolarized cells as it reflects higher numbers of green signal events (JC-1 monomers dominating in depolarized cells) and/or reduced red signal events (JC-1 aggregates dominating in polarized mitochondria).

Mitochondria isolation

A549 and A549 PGAM5-KO cells were grown in 175 cm² cell culture flasks and treated with either bleomycin 100 µg/ml, bleomycin 200 µg/ml or left untreated as controls. After 24 h of bleomycin treatment, cells were harvested using a cell scraper. Mitochondria isolation was then performed as previously described [23]. In brief, dounce homogenization of the harvested cells was performed and the mitochondrial fraction was isolated using differential centrifugation. After obtaining purified mitochondria, protein isolation and immunoblotting were performed as described in the section "immunoblotting".

Mitochondrial reactive oxygen species measurement (mitoSOX, flow cytometry)

A549 and A549 PGAM5-KO cells were treated with either bleomycin 100 µg/ml, bleomycin 200 µg/ml or left untreated as controls. After 24 h cells were stained with mitoSOX red mitochondrial superoxide indicator (M36008, Molecular Probes, Invitrogen) and analyzed with flow cytometry in the BD Accuri C6 (BD Biosciences) or the BD LSR Fortessa (BD Biosciences). Analysis of the data was performed using FlowJoV10 Software (FlowJo LLC).

Statistics

Comparisons among multiple groups were performed using ANOVA as outlined in the particular experiment with Tukey's test as post hoc test. Data sets are displayed as Tukey boxplots (box from 25th to 75th percentile, line represents median; whiskers according to Tukey's method) unless indicated otherwise and statistical significance was accepted with $p < 0.05$ (NS $p \geq 0.05$; *$p < 0.05$; **$p < 0.01$; ***$p < 0.001$). All p values calculated using Tukey's test are given as multiplicity adjusted p values. Statistical calculations were performed using GraphPad Prism 7 (GraphPad Software).

Transient transfection

Transient transfection of A549 PGAM5-KO cells was performed using the Lipofectamine LTX & PLUS Reagent (15338100, Thermo Fisher Scientific) according to the manufacturer's protocol.

For the respective experiments shown in figure 2, A549 PGAM5-KO cells were transfected with PGAM5 or subjected to a transfection control and then subsequently treated with bleomycin 100 µg/ml for 48 h. The PGAM5 plasmid was a kind gift from Prof. Jürgen Behrens. Effective expression of PGAM5 after transfection was proven by immunoblotting.

Transmission electron microscopy (TEM)

A549 and A549 PGAM5-KO cells were either treated with bleomycin or left untreated as controls. After 48 h, cells were fixed using a High Pressure Freezing and Freeze Substitution protocol (0.1% Os/ 0.1% Uac/ 2.5% H_2O/ Acetone). All samples were embedded in Epon, cut to 50 nm and

imaged with the EM910/912 on image-plates. Studies were performed by the Central Unit Electron Microscopy of the German Cancer Research Center (dkfz).

xCELLigence

Proliferation analysis was performed using the xCELLigence DP system. Cells were seeded into E-Plate 16 format wells and allowed to become attached overnight. Treatment was performed with bleomycin 100 µg/ml with untreated cells serving as controls. Measurement intervals were 15 min with an overall measurement period of 48 h after the start of the treatment. The xCELLigence device allows a non-invasive longitudinal assessment of cell monolayer properties by using electrical impedance measurements. Hence, the gathered information facilitates deductive conclusions about cell properties such as morphology, proliferation, and attachment.

Acknowledgements We thank Prof. J. Behrens (Lehrstuhl für Experimentelle Medizin II, Friedrich-Alexander-Universität Erlangen-Nürnberg) for providing the PGAM5 plasmid, Dr. T. Chiriac, Dr. S. Wirtz and Prof. M. von Knebel Doeberitz for supplying material. We thank H. Dorner, G. Förtsch, R. Mehr, S. Rößler, V. Thonn, S. Wallmüller, and A. Wandersee for excellent technical assistance. We thank Dr. M. Neßling for her contribution to the TEM studies.

Author contribution I.G., M.F.N. and C.B. designed the research. I.G., G.-W.H., C.G., E.-S.P., K.R., R.J.R. and D.M. performed the experiments. I.G., M.F.N. and C.B. analyzed the data and wrote the paper. The authors have declared that no conflict of interest exists.

Funding This study was supported by funding from the DFG project BE3686/2, research unit FOR2438, SFB1181, SFB796, SPP1656, and clinical research unit KFO257. The Interdisciplinary Center for Clinical Research (IZKF) Erlangen supported I.G. with a laboratory rotation grant and through participation in the Clinician Scientist Program and C.G. with a funding grant (Project A75).

Compliance with ethical standards

Conflict of interest We, the authors, have no conflicting financial interests.

References

1. King TE Jr, Tooze JA, Schwarz MI, Brown KR, Cherniack RM (2001) Predicting survival in idiopathic pulmonary fibrosis: scoring system and survival model. Am J Respir Crit Care Med 164:1171–1181. https://doi.org/10.1164/ajrccm.164.7.2003140
2. Aggarwal S, Mannam P, Zhang J (2016) Differential regulation of autophagy and mitophagy in pulmonary diseases. Am J Physiol Lung Cell Mol Physio 311:L433–452. https://doi.org/10.1152/ajplung.00128.2016
3. Ryter SW, Choi AM (2015) Autophagy in lung disease pathogenesis and therapeutics. Redox Biol 4:215–225. https://doi.org/10.1016/j.redox.2014.12.010
4. Choi AM, Ryter SW, Levine B (2013) Autophagy in human health and disease. N Engl J Med 368:651–662. https://doi.org/10.1056/NEJMra1205406
5. Mizumura K et al (2014) Mitophagy-dependent necroptosis contributes to the pathogenesis of COPD. J Clin Investig 124:3987–4003. https://doi.org/10.1172/JCI74985
6. Larson-Casey JL, Deshane JS, Ryan AJ, Thannickal VJ, Carter AB (2016) Macrophage Akt1 kinase-mediated mitophagy modulates apoptosis resistance and pulmonary fibrosis. Immunity 44:582–596. https://doi.org/10.1016/j.immuni.2016.01.001
7. Bueno M et al (2015) PINK1 deficiency impairs mitochondrial homeostasis and promotes lung fibrosis. J Clin Investig 125:521–538. https://doi.org/10.1172/JCI74942
8. Patel AS et al (2015) Epithelial cell mitochondrial dysfunction and PINK1 are induced by transforming growth factor-beta1 in pulmonary fibrosis. PLoS One 10:e0121246. https://doi.org/10.1371/journal.pone.0121246
9. Lu W et al (2014) Genetic deficiency of the mitochondrial protein PGAM5 causes a Parkinson's-like movement disorder. Nat Commun 5:4930. https://doi.org/10.1038/ncomms5930
10. Lu W et al (2016) Mitochondrial protein PGAM5 regulates mitophagic protection against cell necroptosis. PLoS One 11:e0147792. https://doi.org/10.1371/journal.pone.0147792
11. He GW et al (2017) PGAM5-mediated programmed necrosis of hepatocytes drives acute liver injury. Gut 66:716–723. https://doi.org/10.1136/gutjnl-2015-311247
12. Holze C et al (2017) Oxeiptosis, a ROS-induced caspase-independent apoptosis-like cell-death pathway. Nat Immunol. 10:10. https://doi.org/10.1038/s41590-017-0013-y
13. Cloonan SM, Choi AM (2016) Mitochondria in lung disease. J Clin Investig 126:809–820. https://doi.org/10.1172/JCI81113
14. Park YS, Choi SE, Koh HC (2018) PGAM5 regulates PINK1/Parkin-mediated mitophagy via DRP1 in CCCP-induced mitochondrial dysfunction. Toxicol Lett 284:120–128. https://doi.org/10.1016/j.toxlet.2017.12.004
15. Hawk MA et al (2018) RIPK1-mediated induction of mitophagy compromises the viability of extracellular-matrix-detached cells. Nat Cell Biol 20:272–284. https://doi.org/10.1038/s41556-018-0034-2
16. Kim SJ et al (2016) Mitochondrial catalase overexpressed transgenic mice are protected against lung fibrosis in part via preventing alveolar epithelial cell mitochondrial DNA damage. Free Radical Biol Med 101:482–490. https://doi.org/10.1016/j.freeradbiomed.2016.11.007
17. Gomes LC, Scorrano L (2011) Mitochondrial elongation during autophagy: a stereotypical response to survive in difficult times. Autophagy 7:1251–1253. https://doi.org/10.4161/auto.7.10.16771
18. Rambold AS, Kostelecky B, Elia N, Lippincott-Schwartz J (2011) Tubular network formation protects mitochondria from autophagosomal degradation during nutrient starvation. Proc Natl Acad Sci USA 108:10190–10195. https://doi.org/10.1073/pnas.1107402108
19. Moriwaki K et al (2016) The mitochondrial phosphatase PGAM5 is dispensable for necroptosis but promotes inflammasome activation in macrophages. J Immunol 196:407–415. https://doi.org/10.4049/jimmunol.1501662
20. Matute-Bello G et al (2011) An official American Thoracic Society workshop report: features and measurements of experimental acute lung injury in animals. Am J Respir Cell Mol Biol 44:725–738. https://doi.org/10.1165/rcmb.2009-0210ST
21. Ashcroft T, Simpson JM, Timbrell V (1988) Simple method of estimating severity of pulmonary fibrosis on a numerical scale. J Clin Pathol 41:467–470

22. Schindelin J, Arganda-Carreras I, Frise E, Kaynig V, Longair M, Pietzsch T et al (2012) Fiji: an open-source platform for biological-image analysis. Nat Methods 9:676–682
23. Frezza C, Cipolat S, Scorrano L (2007) Organelle isolation: functional mitochondria from mouse liver, muscle and cultured fibroblasts. Nat Protoc 2:287–295. https://doi.org/10.1038/nprot.2006.478